Combined Partial Oxidation of Methane to Synthesis Gas and Production of Hydrogen or Carbon Monoxide in a Fluidized Bed using Lattice Oxygen

Journal Article

Author(s):
Donat, Felix (iD); Xu, Yongqing; Müller, Christoph R.

Combined partial oxidation of methane to synthesis gas and production of hydrogen or carbon monoxide in a fluidized bed using lattice oxygen

Felix Donat[a], Yongqing Xu[a,b], Christoph R. Müller[a,*]

[a] Laboratory of Energy Science and Engineering, Department of Mechanical and Process Engineering, ETH Zürich, Leonhardstrasse 21, 8092 Zürich, Switzerland

[b] State Key Laboratory of Coal Combustion, School of Energy and Power Engineering, Huazhong University of Science and Technology, 1037 Luoyu Road, Wuhan 430074, China

* Corresponding author. E-mail address: muelchri@ethz.ch (Christoph R. Müller)

Abstract

Perovskite-based oxygen carriers have shown promise for the partial oxidation of methane in fixed bed reactors, but they have not been investigated in detail in bubbling fluidized bed reactors, where bypassing of the methane and backmixing of the product gas can occur. Using a Lanthanum strontium ferrite ($La_{0.85}Sr_{0.15}FeO_3$) as the oxygen carrier, it is demonstrated that excellent performance can be achieved in a fluidized bed reactor for both the partial oxidation of methane during reduction of the oxygen carrier and the carbon dioxide or water splitting reactions during re-oxidation of the oxygen carrier in a chemical looping fashion. The effective oxygen storage capacity is > 10 wt.%, allowing to produce > 6 mol of synthesis gas with a ratio of hydrogen to carbon monoxide slightly below 2 during partial oxidation, and > 6 mol of carbon monoxide or hydrogen during re-oxidation per kg oxygen carrier in a complete redox cycle. The selectivity towards synthesis gas is > 99% and the conversion of carbon dioxide to carbon monoxide (or steam to hydrogen) is ~ 97% (or ~ 94%) at temperatures > 900°C.

Introduction

The efficient conversion of CH_4 to a synthesis gas (a mixture of H_2 and CO) via reforming reactions (such as the dry reforming of methane, DRM, or the steam reforming of methane, SRM) or its partial oxidation, POx, require catalysts, which are often expensive or toxic, or both. POx can be performed also non-catalytically but demands high reaction temperatures (for a CH_4 conversion of > 99%, reaction temperatures > 1000°C at 1 atm or > 1450°C at 50 atm are needed). Depending on the reaction scheme, different ratios of H_2 to CO (ranging from 1:1 for DRM to 3:1 for SRM) can be expected in the product gas, which may be used directly in downstream chemical production processes, e.g. Fischer-Tropsch synthesis. For the partial oxidation of CH_4 ($CH_4 + 0.5\,O_2 \rightarrow 2\,H_2 + CO$), a supply of O_2 is needed, which is a main contributor to the operating costs of the process [1,2]. Instead of using gaseous O_2, it has been proposed to use lattice oxygen of metal oxides to convert CH_4 into a synthesis gas [3,4], and this has been termed chemical looping reforming [5]. The principal idea is to keep the oxygen to fuel ratio low to prevent the fuel from being fully oxidized to CO_2 and H_2O [6–8], allowing to use a wide range of metal oxide-based oxygen carrier, e.g. NiO or Mn_2O_3. Some metal oxides naturally convert CH_4 to synthesis gas (instead of combusting it) owing to their thermodynamic properties, e.g. La-Fe-based perovskites [9–12]. In this class of materials, to improve reactivity and selectivity towards synthesis gas, doping of the A-site (La) of the perovskite with Sr has mostly been employed [13–15], but also the partial substitution of the Fe

on the B-site with Mn [16], Al [17] or Cr [18] has been reported to have a positive effect on the partial oxidation performance. La-(Sr)-Fe-based perovskites do not only possess beneficial thermodynamic properties for the partial oxidation of CH_4, but also, once a fraction of the lattice oxygen has been consumed, for the splitting of CO_2 (or H_2O) to generate CO (or H_2). Hence, this class of materials is often investigated for combined partial oxidation and CO_2 (or H_2O) splitting reaction schemes [19–22]. Subject to the oxidant used, the sum of the two reaction half steps is equivalent to the DRM (with CO_2 as oxidant) or SRM (with H_2O as oxidant), where from CH_4 and the oxidant a synthesis gas with a ratio of H_2 to CO of 1:1 or 3:1 is produced; often such schemes are referred to as chemical looping reforming. The thermodynamic properties of perovskites vary as function of A- or B-site substitution and non-stoichiometry in lattice oxygen. The perovskite system in general is very well understood and characterized [23–25], but for most applications, a reduction beyond the perovskite structure is not considered, thus utilizing only a fraction of the theoretical amount of redox-active lattice oxygen [26–29]. In this work, we do not report on the development of new perovskite-based oxygen carriers, but use a well-known La-Sr-Fe-O system, specifically $La_{0.85}Sr_{0.15}FeO_3$, as oxygen carrier and investigate its performance for partial oxidation of CH_4 and the subsequent splitting of CO_2 (or H_2O) to maximize the utilization of the material's redox-active lattice oxygen. While several other studies have shown good results with similar materials in membrane [30] or fixed bed reactors [31–33], only a few studies have employed fluidized bed reactors [34–36]. We demonstrate that an excellent performance of $La_{0.85}Sr_{0.15}FeO_3$ can be achieved in a fluidized bed reactor for both the partial oxidation of CH_4 and the splitting reaction, while potentially eliminating the use of O_2/air entirely. The effective oxygen storage capacity was > 10 wt.%, equivalent to a production of > 6 mol of synthesis gas during reduction and > 6 mol of CO or H_2 during re-oxidation per kg of oxygen carrier (note that 0.1 kg of lattice oxygen per kg oxygen carrier corresponds to 3.125 mol of O_2).

Experimental

The perovskite-based $La_{0.85}Sr_{0.15}FeO_{3-\delta}$ oxygen carrier particles (for simplicity, the formula $La_{0.85}Sr_{0.15}FeO_3$ is used to denote the oxygen carrier in most instances) were synthesized from nitrates using a modified Pechini-method, followed by granulation and calcination at 1250°C. The material was characterized using X-ray diffraction (XRD), electron microscopy (scanning and transmission electron microscopy, SEM and TEM, with energy-dispersive X-ray spectroscopy, EDX), N_2 sorption, Raman spectroscopy and inductively coupled plasma optical emission spectroscopy (ICP-OES).

The performance of the oxygen carrier for converting CH_4 in a redox fashion was evaluated using a thermogravimetric analyzer and a fluidized bed reactor. The off-gases from both apparatus were sampled continuously and analyzed using infrared, thermal conductivity and paramagnetic analyzers. Details on the experimental methods are available in the Supporting Information (SI).

Table 1: Summary of the experimental conditions in the fluidized bed experiments.

Experimental parameter		# 1	# 2	# 3	# 4	# 5
Temperature (°C)[a]		800 – 950	900	900	900	900 – 950
Pressure (atm)		1	1	1	1	1.4
Reduction step	Atmosphere	8.6 vol.% CH_4	8.6 vol.% CH_4	8.6 vol.% CH_4	8.6 vol.% CH_4	8.6 vol.% CH_4
	Time (s)	900	900	900	900	900
1st Oxidation step	Atmosphere	7.1 vol.% CO_2	7.1 vol.% CO_2	7.0 vol.% steam[b]	7.1 vol.% CO_2	7.1 vol.% CO_2
	Time (s)	600	600	600	600	600
2nd Oxidation step	Atmosphere	85.7 vol.% air	85.7 vol.% air	85.7 vol.% air	-	85.7 vol.% air
	Time (s)	300	300	300	-	300
Total flow (ml min^{-1})		700	525, 700, 875	700	700	700
Comment		Effect of temperature	Effect of total flow rate	Effect of steam	Effect of air oxidation step	Effect of pressure

[a] The actual bed temperature was usually 10 – 15°C higher than the set reactor temperature.
[b] The flow rate of the water pump was set to 2.4 ml h^{-1}.

A summary of the experimental conditions using the fluidized bed, for which particles sieved to 250 – 425 μm were used, is given in Table 1. In all experiments, diluted gas mixtures were used with N_2 being the diluent. More than 80 redox cycles were performed in the fluidized bed, corresponding to more than 50 h of fluidization at high temperature. The reactor and filters were cleaned after every ~ 8 – 10 h of operation. No significant particle breakage, attrition or loss of material was observed, although the granulated particles were not optimized for mechanical stability. No attempts were made to measure the compression strength of the particles, keeping in mind that the compressing strength of oxygen carrier particles can be an important parameter for operation at large scale to estimate their lifetime. The following performance indicators were used on a N_2-free basis:

- *Conversion of CH_4, X_{CH4},* at time $t = 1$ – mole fraction of CH_4 measured in the off-gas / sum of mole fractions of CO, CO_2 and CH_4 measured in the off-gas

$$X_{CH4}(t) = 1 - \frac{x_{CH4}(t)}{x_{CO}(t) + x_{CO2}(t) + x_{CH4}(t)}$$

Eq. 1

- *Selectivity towards synthesis gas, S_{Syngas},* at time t = (sum of mole fractions of CO and H_2 measured in the off-gas) / (sum of mole fractions of CO, H_2, CO_2 and H_2O measured in the off-gas)

$$S_{Syngas}(t) = \frac{x_{CO}(t) + x_{H2}(t)}{x_{CO}(t) + x_{CO2}(t) + x_{H2}(t) + x_{H2O}(t)}$$

Eq. 2

- *Oxygen storage capacity, R_{OC}* = (mass of initial oxidized oxygen carrier – mass of oxygen carrier when all redox-active lattice oxygen has been consumed) / (mass of initial oxidized oxygen carrier)

$$R_{OC} = \frac{m_{ox} - m_{red}}{m_{ox}}$$

Eq. 3

- *Lattice oxygen conversion, $X_{[O]}$,* at time t = (moles of lattice oxygen consumed) / (total moles of redox-active lattice oxygen in the oxygen carrier)

$$X_{[O]}(t) = \frac{\int_{t_0}^{t} n_{O2} \cdot dt}{n_{O2,OC}} = \int_{t_0}^{t} \frac{X_{CH4,Feed}(t) \cdot (x_{CO}(t) + x_{H2O}(t)) + x_{CO2}(t))}{x_{CO}(t) + x_{CO2}(t) + x_{CH4}(t)} \cdot \dot{n}_{tot,Feed} \cdot dt \cdot \frac{1}{n_{O2,OC}}$$

Eq. 4

where $\dot{n}_{tot,Feed}$ is the total molar flow rate of gas entering the reactor

- *Ratio of H_2 to CO, R,* at time t = (mole fraction of H_2 measured in the off-gas) / (mole fraction of CO measured in the off-gas)

$$R = \frac{x_{H2}(t)}{x_{CO}(t)}$$ Eq. 5

- *Conversion of CO_2 to CO, X_{CO2},* at time t = (mole fraction of CO measured in the off-gas) / (sum of mole fractions of CO and CO_2); the conversion of steam to H_2 was calculated equivalently.

$$X_{CO2}(t) = \frac{x_{CO}(t)}{x_{CO}(t) + x_{CO2}(t)}$$ Eq. 6

Average values were computed for the time span of the true partial oxidation period, i.e. after non-selective lattice oxygen was consumed for the combustion of CH_4 and the selectivity towards synthesis gas was > 99% until the end of the reduction step.

Results and Discussion

Material development

The initial material development focused on a wide range of Sr-Fe-based perovskites with various degrees of substitution of the A- and B-sites; the detailed discussion of these results is beyond the scope of the present work. Briefly, from TGA experiments it was found that substitution of Sr with La was necessary for high reactivity and high selectivity towards synthesis gas (i.e. a mixture of CO and H_2). The optimum substitution of La with Sr was found to range between 0.1 and 0.2, in agreement with results reported in the literature [37]. Higher reactivity for CH_4 oxidation with a higher degree of substitutions of La by Sr was not observed [38,39]. Resistance towards sintering could be improved by partially substituting Fe (B-site of the perovskite) with Cr at the expense of a lowered oxygen storage capacity, whereas substitution with Co or Mn improved the resistance towards coking. Partial substitution of Fe with Al improved the oxygen carrier's reactivity for the conversion of CH_4, but also increased its tendency for coking, in contrast to what has been reported elsewhere [40]. Despite the beneficial effects the B-site substitutions had, it was relatively tedious to obtain phase-pure perovskites owing to the differences in ionic radii that would prevent its stable incorporation in the perovskite lattice following Goldschmidt's geometrical considerations [41]. Many materials thus contained mixtures of spinel and perovskite, which ultimately resulted in a reduced selectivity towards synthesis gas. The oxygen carrier of choice was $La_{0.85}Sr_{0.15}FeO_3$, because it showed the most stable performance in the fluidized bed experiments with no significant phase changes upon redox cycling; this is discussed in detail below.

TGA experiments

Investigation of the performance of the oxygen carrier for the partial oxidation of CH_4 was carried out initially in a TGA at 850°C (note that the actual sample temperature was ~ 3 – 5°C lower than the setpoint). The off-gas from the TGA was sampled and analyzed continuously to determine the selectivity towards synthesis gas. The conversion of CH_4 in the TGA experiments was always very low due to the cantilever-type balance arm with the reactive gas flowing horizontally over the sample; thus, most of the gas was not in contact with the oxygen carrier inside the crucible and left the TGA reaction chamber unconverted.
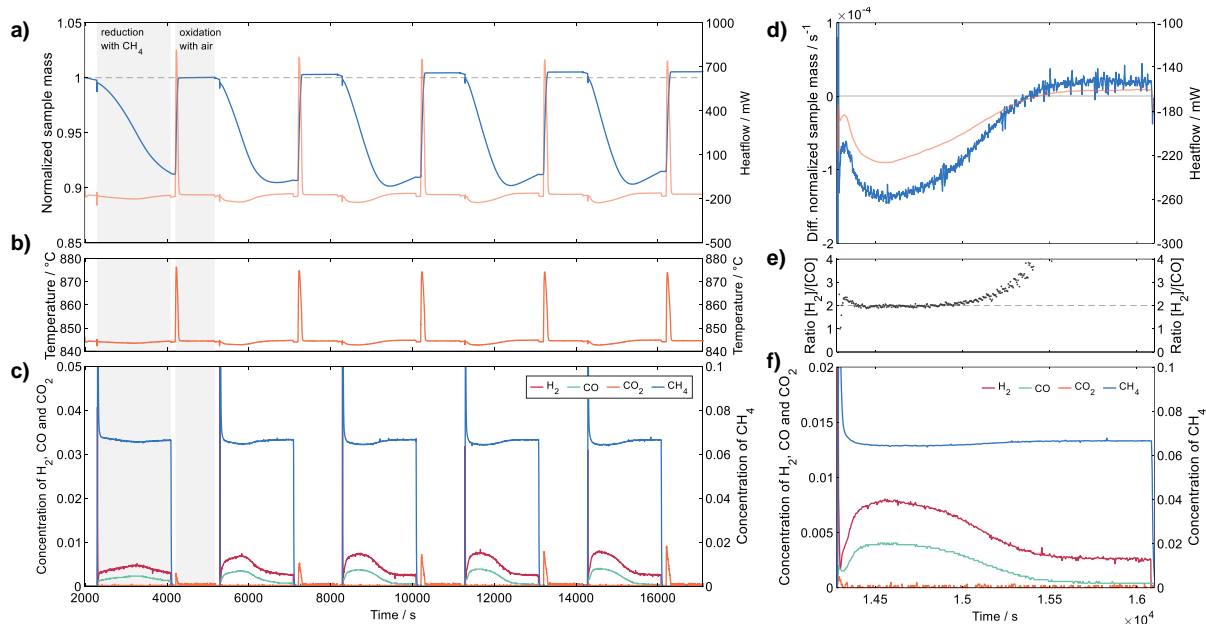
Figure 1: Results from a TGA experiment performed at 850°C using CH_4 during reduction and air during oxidation with fresh $La_{0.85}Sr_{0.15}FeO_3$. a) – c) show the normalized sample mass, heatflow, temperature and gas concentrations recorded during the first five reaction cycles. d) – f) focus on the 5th reduction showing the 1st derivative of the normalized sample mass, heatflow, ratio of $[H_2]/[CO]$ and gas concentrations.

Figure 1 summarizes the results from a typical TGA experiment when the oxygen carrier $La_{0.85}Sr_{0.15}FeO_3$ was reduced in CH_4 and oxidized in air. Figure 1 a) – c) show the recorded sample mass, heatflow, temperature and gas concentrations for the first five reaction cycles (note that the term "gas concentration" in this work is equivalent to "mole fraction" and is thus reported without units). From the normalized sample mass, plotted in Figure 1 a), at the end of the reduction step, it can be seen that the oxygen carrier "activated" with cycling. The increase in sample mass after the local minimum implies that coking occurred, which was confirmed by Raman spectroscopy when analyzing a sample collected after reduction (shown in Figure S9 in the SI). These carbon deposits were burned in the subsequent oxidation step with air, resulting in the production of CO_2, as seen in Figure 1 c). The magnitude of the CO_2 peaks at the beginning of the oxidation step increased with cycle number, because more carbon was deposited on the oxygen carrier's surface during reduction. With activation of the oxygen carrier, the extent of reduction (i.e. the consumption of lattice oxygen) increased, leaving more time for coking to occur. CO_2 was generated also during the first re-oxidation step, although this was not directly apparent from the change of sample mass. The change of sample mass during reduction thus reflected overlaying effects of lattice oxygen consumption (mass decrease) and coking due to the decomposition of CH_4 (mass increase), with the latter being more significant for high oxygen carrier conversions. Interestingly, the sample mass after oxidation increased with cycling beyond the sample mass of the as-synthesized material, suggesting additional uptake of oxygen.

On an oxide basis, $La_{0.85}Sr_{0.15}FeO_3$ consists of 59.2 wt% La_2O_3, 6.6 wt% SrO and 34.2 wt% Fe_2O_3. Considering these three components separately for the purpose of lattice oxygen estimation, only Fe_2O_3 is reducible under the conditions of the TGA experiments, giving a theoretical oxygen storage capacity of 10.3 wt% O_2 per g oxygen carrier. The oxygen storage capacity of the oxygen carrier after the 5th reaction cycle was 10.6 wt.% (after correcting for carbon produced) and was thus in good agreement with only lattice oxygen from "Fe_2O_3" being redox-active.

Both the heatflow and temperature measurements in Figure 1 a) and b) show that the reduction of the oxygen carrier with CH_4 was endothermic and that the re-oxidation with air was strongly exothermic. This is different from the conventional partial oxidation of CH_4 with O_2 co-fed, which is an exothermic reaction. Despite the large increase in sample temperature, no sintering/agglomeration of the oxygen carrier powder was observed when collecting it after the cycling experiment and the oxygen carrier powder could easily be pulverized by moving it gently between fingers.

Figure 1 d) – f) focus in detail on the 5th reduction step. The heatflow and temperature profiles in Figure 1 d) indicate that most of the reduction of the oxygen carrier occurred in a single, endothermic step. However, at the very beginning of the reduction reaction (within the first ~ 20 s), a local maximum in the heatflow curve was observed, in line with small amounts of CO_2 being produced Figure 1 f)). CH_4 was thus combusted before being partially oxidized to a synthesis gas by the oxygen carrier; this observation will become clearer in the discussion of the results from fluidized bed experiments below. During the production of a synthesis gas, no CO_2 was measured in the off-gas from the TGA (Figure 1 f)), yielding a selectivity towards synthesis gas > 99%. The ratio of H_2 to CO was close to 2, as expected from thermodynamic considerations and previous observations made in other studies [10,17]. After ~ 720 s into the reduction, the ratio of H_2 to CO increased to values > 2 due to the cracking of CH_4 with the simultaneous production of H_2 and carbon.

Another series of cycling experiments was performed using CO_2 as the only oxidant in the oxidation step; the results are shown in Figure S1 in the SI. The sample mass was always regenerated completely after oxidation with CO_2 in a mildly exothermic reaction, i.e. no strong increase in temperature was observed during oxidation, in contrast to the experiment where the oxidation step was carried out in air. The measured oxygen storage capacity was ~ 9.9 wt.% and thus only slightly lower than when the material was oxidized in air. In the experiment shown in Figure S1, an "activated" oxygen carrier was used that had been cycled in the fluidized bed before, thus explaining the higher tendency for coking. Otherwise, no significant differences were observed during reduction compared to the experiment where air was used in the oxidation step.

Fluidized bed experiments

Figure 2 presents the results from an experiment using the fluidized bed reactor at 900°C; in a) gas concentrations measured in the off-gas from the reactor are shown for a complete reaction cycle, and in b) the corresponding bed temperature and pressure are shown. Figure 2 c) – f) focus on the reduction step only. Similar plots for cyclic experiments performed at 800°C, 850°C and 950°C are shown in Figures S2 – S4 in the SI.
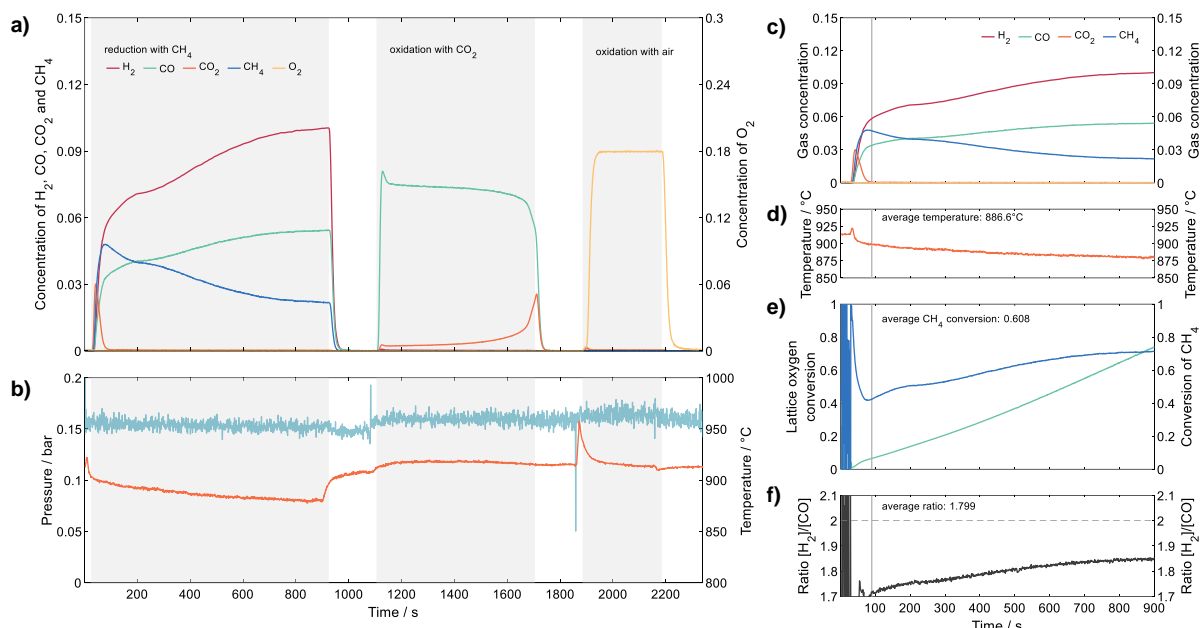
Figure 2: Results from a fluidized bed experiment performed at 900°C using CH_4 for reduction and CO_2 and air, respectively, during the two oxidation steps using ~ 7.5 g of $La_{0.85}Sr_{0.15}FeO_3$. a) and b) show the gas concentrations, pressure and bed temperature recorded during a complete reaction cycle. c) – f) focus on the reduction step showing the gas concentrations, bed temperature, lattice oxygen conversion, conversion of CH_4 and the ratio of $[H_2]/[CO]$. Note that for a direct comparison of the off-gas and temperature measurements, the temperature curve was shifted in time by 25 s. The grey vertical line indicates when $[CO_2]$ falls below 0.1% and the selectivity towards synthesis gas was > 99%.

Similar to the gas profiles observed in the TGA experiments, CO_2 was produced at the beginning of the reduction step due to the combustion of CH_4 with lattice oxygen from the oxygen carrier (this was verified through blank experiments and using a humidity sensor, with which a ratio of H_2O to CO_2 of ~ 2 was measured), causing an increase in bed temperature (Figure 2 c) and d)). Subsequently, there was a sharp transition to partial oxidation with only very small amounts of CO_2 (< 0.05 vol.%) and steam (~ 0.2 – 0.3 vol.%) present in the off-gas (the steam concentration is not shown in Figure 2). The selectivity towards synthesis gas in the partial oxidation regime was always > 99%. Note that the shape of the gas profiles was affected by gas mixing effects downstream of the bed in the sampling system, resulting in an overlap of CO_2 and synthesis gas. Owing to the endothermicity of the partial oxidation reaction, the bed temperature decreased by more than 30°C. The conversion of CH_4 increased during that time from 42% to 71%, implying that the formation of oxygen vacancies during reduction had a larger effect on the material's activity than the reaction temperature [42]. Interestingly, contrary to observations made in the TGA experiments, the ratio of H_2 to CO was < 2 throughout the reduction reaction and increased with increasing conversion of CH_4. Figure 2 e) shows that the total consumption of redox-active lattice oxygen during reduction was ~ 75%, whereby ~ 7% of the total redox-active lattice oxygen was consumed at the very beginning for the combustion of CH_4 and was hence non-selective for partial oxidation.

Turning to the oxidation steps, it is apparent from Figure 2 a) that most of the CO_2 was converted to CO. The conversion of CO_2 to CO in this experiment was ~ 97% prior breakthrough and varied only marginally with the amount of lattice oxygen recovered. Even though the oxygen carrier was largely re-oxidized with CO_2 (~ 88% of the lattice oxygen converted during reduction was replenished by oxidation with CO_2), the second oxidation step with air resulted in a considerable increase in temperature of the bed. At the highest temperature studied (reactor set temperature of 950°C), the bed temperature peaked at 1085°C. The oxidation reaction in air was fast and limited by the supply of oxygen.

The results of the fluidized bed experiments are summarized in the bar charts in Figure 3 a) – f). Average values reported in Figure 3 a) – c) were determined for the average temperatures shown in Figure 3 d).
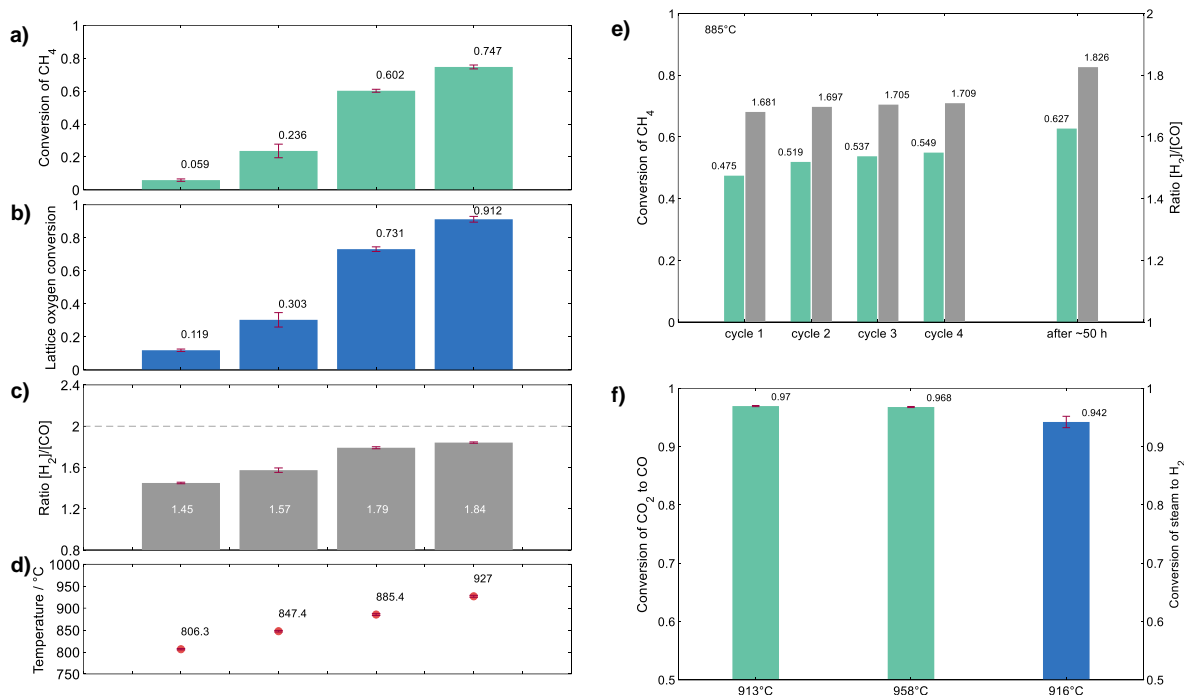

Figure 3: Summary of the results from the fluidized bed experiments of series #1 and #3 in Table 1. a) – c) show the average conversion of CH_4, average lattice oxygen conversion and average ratio of $[H_2]/[CO]$ for the average bed temperatures plotted in d). In e), the conversion of CH_4 and the corresponding ratio of $[H_2]/[CO]$ are plotted for four consecutive reaction cycles at an average bed temperature of 885°C when the oxygen carrier was still activating; for comparison, values obtained for the fully activated oxygen carrier are shown. In f), the conversions of CO_2 to CO and steam to H_2 are compared for different temperatures. Error bars represent two standard deviations based on measurements from at least five reaction cycles.

The average conversion of CH_4 increased with temperature without noticeably affecting the selectivity towards synthesis gas. The activation of the oxygen carrier observed in the TGA was also seen in the fluidized bed experiments: Figure 3 e) shows that the average conversion of CH_4 increased over the first four reaction cycles at 885°C (reactor set temperature of 900°C) and was still much lower than that of the fully activated material after ~ 50 h of cycling in the fluidized bed; note that no significant change in activity of the oxygen carrier was observed after ~ 15 h of cycling in the fluidized bed.

The lattice oxygen conversion was determined at the end of the reduction period (after 900 s) and was found to increase with conversion of CH_4. The ratio of H_2 to CO measured was directly related to the conversion of CH_4, as can also be seen by comparing Figure 2 e) and f). A ratio of H_2 to CO < 2 implies that one or more side reactions occurred where H_2 was consumed and, or, CO was produced. For the La-Sr-Fe-based oxygen carrier this is only possible in a reactor where backmixing of product gas can occur, such as a fluidized bed. One possible side reaction is the reverse water-gas shift reaction (rWGS, $CO_2 + H_2 \rightarrow CO + H_2O$), which is thermodynamically favored at the temperatures investigated in this work with an equilibrium constant of unity at ~ 820°C. The decomposition of CH_4 ($CH_4 \rightarrow C + 2H_2$) can be ruled out as a major side reaction because it would increase the ratio of H_2 to CO. The synthesis gas produced through the partial oxidation of CH_4 reacts with the oxygen carrier particles to produce CO_2 and steam, which in turn could react with the synthesis gas following the rWGS reaction, or re-oxidize the partially reduced oxygen carrier to generate synthesis gas again. Since the rWGS reaction is favored at higher temperatures, one would expect to observe lower

ratios of H_2 to CO with increasing temperature. From the results in Figure 3 a) – d) it appears the ratio was more correlated with the conversion of CH_4 than the actual bed temperature. In addition, experiments with varying total flow rates (series #2 in Table 1, the results are presented in Figure S5 in the SI) showed that longer gas-solid contact times (i.e. lower gas flow rates) resulted in larger ratios of H_2 to CO, whereas shorter gas solid contact times (i.e. larger gas flow rates) resulted in lower ratios of H_2 to CO. These results, together with the fact that during the partial oxidation stage the concentration of steam measured in the off-gas was more than four times higher than that of CO_2, suggest that the rWGS reaction was not ultimately determining the final product gas composition and that dynamic reduction/oxidation reactions of the gas species with the oxygen carrier were also important.

Conventional partial oxidation of CH_4 with O_2 co-feed is thermodynamically favored at low pressure due to volume expansion; increasing the pressure at a given temperature will therefore lower the conversion of CH_4. Similar effects were expected to occur when using lattice oxygen as oxidant. Unfortunately, the maximum pressure of the fluidized bed was limited to ~ 0.4 bar above atmosphere. The results are presented in Figure S6 in the SI and show that the average bed temperature was lower than under atmospheric conditions due to the higher gas density and the higher extent of reduction, making a direct performance comparison with atmospheric conditions difficult. The average conversion of CH_4 was ~ 0.6 at elevated pressure, which was comparable with the values measured at ambient pressure (Figure 3 a)). Interestingly, the average ratio of H_2 to CO was higher than at atmospheric pressure, suggesting that side reactions were suppressed.

Figure 3 f) compares the conversion of CO_2 to CO measured during the oxidation step with CO_2 as a function of temperature; in addition, experiments were performed using steam as the oxidant to determine the conversion of steam to H_2. The conversion CO_2 to CO was ~ 97% for average bed temperatures of 913 and 958°C and was not affected by elevated pressure. At lower set reactor temperatures of 800 and 850°C, the conversion CO_2 to CO varied somewhat with the amount of lattice oxygen recovered, from ~ 97% after 60 s to ~ 86% after 240 s (Figure S3 in the SI). Experiments performed with steam as oxidant at an average bed temperature of 916°C gave conversions of steam to H_2 of ~ 94%, which was much higher than what "conventional" oxygen carrier materials, e.g. Fe_2O_3, achieve thermodynamically in chemical looping H_2O splitting schemes [20,43]. The H_2 produced had a purity > 98.5% on a steam- and N_2-free basis, with CO being the only measurable contaminant at the very beginning of the oxidation reaction (Figure S7 in the SI). From the amount of CO produced during the steam oxidation step via gasification, the total amount carbon deposited on the oxygen carrier during reduction was < 130 µg per g oxygen carrier at all temperatures studied, which was too little to be detected by XRD or Raman spectroscopy ((Figure 4 a) and Figure S9). Importantly, performing the H_2O (or CO_2) splitting reaction using La-Sr-Fe-based perovskites, such as $La_{0.85}Sr_{0.15}FeO_3$, can alleviate the conceptual drawbacks that fluidized beds have for H_2O splitting over e.g. counter-current moving bed reactors [44,45]. This is because reduction and oxidation occur in a single reaction step, providing a constant production rate of H_2 (or CO), with no additional thermodynamic limitations due to further phase transitions. With 1 kg of $La_{0.85}Sr_{0.15}FeO_3$, > 6 mol of H_2 (or CO) can be generated at nearly complete conversion.

Another potential advantage of this class of oxygen carriers is the regenerability of lattice oxygen using CO_2 (or steam) only, without requiring a separate oxidation step by air. One complete redox cycle is shown in Figure S8 in the SI, from which it is also apparent that the extent of the initial combustion of CH_4 was reduced. Only ~ 1% of the total theoretical redox-active lattice oxygen was consumed for the combustion of CH_4 compared to ~ 7% when an additional air oxidation step was included in a full reaction cycle. It is important to note that the

regeneration of lattice oxygen with air generates a large amount of heat that could potentially be utilized within the process, e.g. to balance the endothermicity of the partial oxidation reaction. Nonetheless, re-oxidizing the reduced oxygen carrier particles directly with air increases their temperature by several hundred degrees and potentially results in the defluidization of the bed, which would terminate operation immediately.

Material characterization

The perovskite $La_{0.85}Sr_{0.15}FeO_{3-\delta}$ is a non-stoichiometric material that can store or release lattice oxygen without undergoing bulk phase changes, subject to oxygen partial pressure and temperature. The parameter δ takes theoretically values between 0 and 0.5, which is reflected by a varying unit cell parameter in the X-ray diffractogram [23].
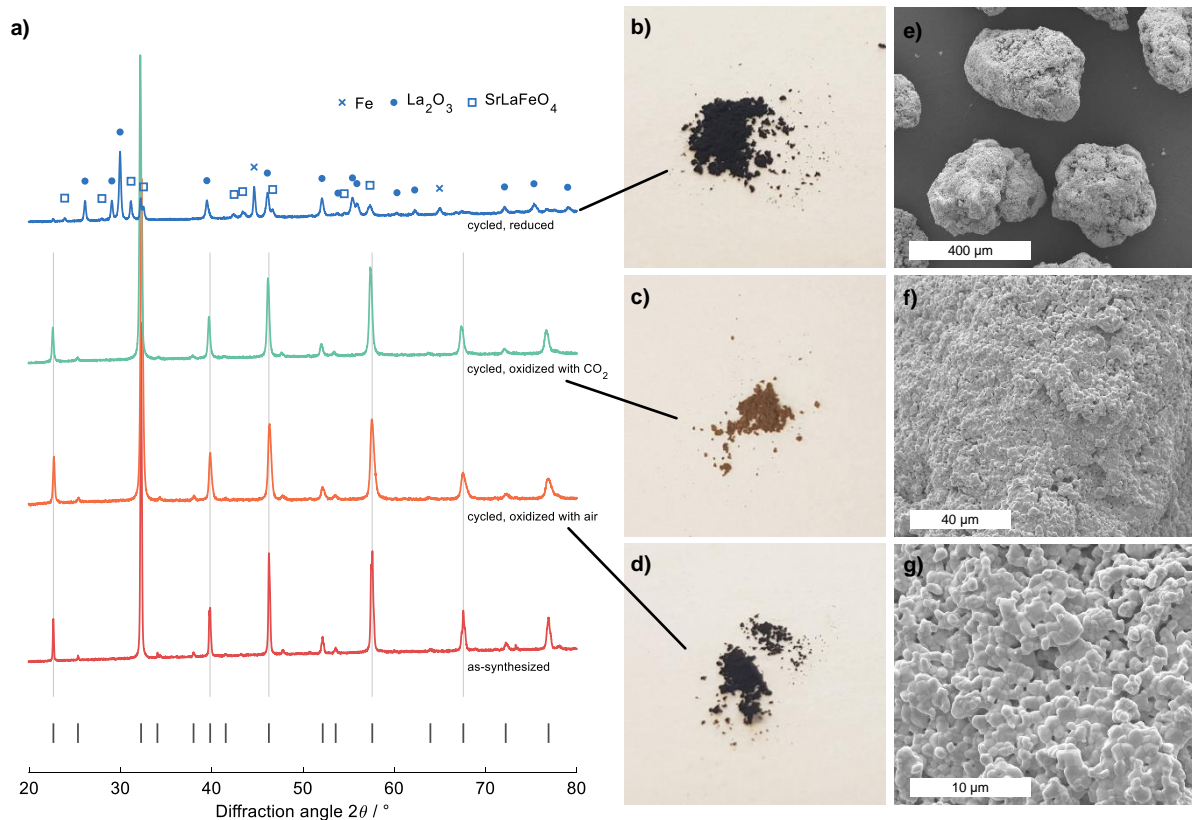

Figure 4: a) XRD pattern obtained for the as-synthesized oxygen carrier, cycled oxygen carrier after oxidation with air, cycled oxygen carrier after oxidation with CO_2, and cycled oxygen carrier after reduction with CH_4. The vertical grey lines indicate the exact peak positions of the pattern for the as-synthesized oxygen carrier. The short lines below the XRD pattern act as reference for phase-pure $La_{0.85}Sr_{0.15}FeO_3$. b) – d) show images of the powders that were analyzed to obtain the diffractograms shown in a). e) – g) show SEM images of the as-synthesized oxygen carrier particles (sieved to 250 – 425 µm) at different magnifications.

Figure 4 a) plots diffractograms obtained for the as-synthesized oxygen carrier, oxygen carrier after ~ 50 h of fluidized bed operation when oxidized with air, oxidized oxygen carrier after ~ 50 h of fluidized bed operation when oxidized with CO_2, and oxygen carrier collected from the fluidized bed after the reduction stage after ~ 45 h of operation. The oxygen carrier was phase-pure and no secondary crystalline phases were found after cycling. Results from TEM with EDX maps of the oxygen carrier oxidized in air (Figure 5) show that all elements were distributed uniformly throughout the sample. Using ICP-OES, the actual molar ratio of La:Sr in the oxygen carrier was 5.0, equivalent to ~ 17% substitution of La with Sr. From the XRD

results in Figure 4 a), a very small shift in peak position towards higher diffraction angles is visible when comparing the diffraction pattern of the as-synthesized oxygen carrier with that of the cycled oxygen carrier oxidized in air. This shift reflects a decrease in δ, corresponding to a greater amount of lattice oxygen stored within the oxygen carrier. The increase in lattice oxygen was also observed in the TGA experiments (Figure 1 a)) during the activation of the oxygen carrier. Upon oxidation with CO_2 only, the principal perovskite phase was recovered, but was depleted in oxygen, as can be seen from the shift in peak position towards lower diffraction angles. In addition, the color changed from dark grey to ocherous (Figure 4 c) and d)). The lower amount of (non-selective) lattice oxygen, i.e. a higher value of δ, in the material agrees well with the results from the fluidized bed, where the contribution of lattice oxygen to the combustion of CH_4 at 900°C was reduced from ~ 7% to ~ 1%. It is also in good agreement with the results from the TGA experiments, where a difference in the amount of redox-active lattice oxygen was observed when re-oxidizing the oxygen carrier in CO_2 or air, which can be explained with a change of δ.

The crystalline phases identified in the diffractogram of the reduced oxygen carrier were Fe, La_2O_3, and a mixed Sr-based Ruddlesden-Popper-phase. No carbide phases were detected as expected, since no appreciable degree of coking was observed in the fluidized bed. Interestingly, results from the fluidized bed suggest that the oxygen carrier was reduced completely, with all redox-active lattice oxygen consumed (equivalent to the fraction of Fe_2O_3 being reduced to metallic Fe). Further, from the EDX maps obtained for the reduced oxygen carrier (Figure 5), Fe and Sr existed spatially separated, which implies that the Ruddlesden-Popper-phase identified by XRD was, in fact, free of Fe.

The oxygen carrier particles (sieved to 250 – 425 µm) used in the fluidized bed reactor were analyzed using SEM. The particles were irregular in shape and composed of micrometer-sized particles, which sintered together upon calcination at high temperature (Figure 4 e) – g)). Both the as-synthesized and cycled oxygen carrier particles had low BET surface areas (< 1 m^2 g^{-1}). The bulk density of the as-synthesized oxygen carrier was ~ 2490 kg m^{-3}, whereas the bulk density of the cycled oxygen carrier was ~ 2430 kg m^{-3} and thus slightly lower. Assuming a void fraction of 0.45 when measuring the bulk density and using mass and volume of the orthorhombic unit cell of the perovskite yields a particle porosity of ~ 0.30. The minimum fluidization velocity U_{mf} of the oxygen carrier particles at 900°C was ~ 5.9 cm s^{-1} (calculated using Wen and Yu's correlation [46]), translating into values for U_0/U_{mf} at 900°C of ~ 4 – 5; the bed was in the bubbling regime in the absence of chemical reactions (here, U_0 is the superficial gas velocity).
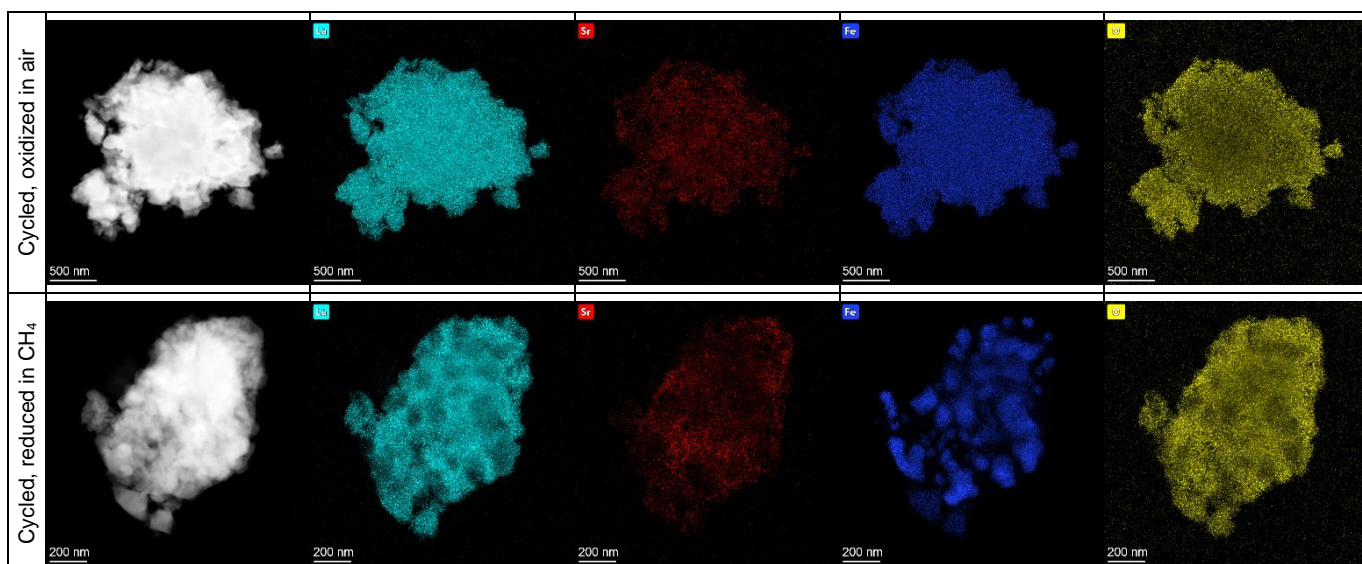
Figure 5: High-angle annular dark-field (HAADF) images and elemental mapping of cycled oxygen carrier oxidized in air, and cycled oxygen carrier reduced in CH₄. The images correspond to the same samples that were analyzed via XRD in Figure 4.

Conclusions

The suitability of perovskite-based La-Sr-Fe-oxides for the partial oxidation of CH_4 and, or, H_2O or CO_2 splitting has been demonstrated before, but most studies have focused on fixed bed operation where no significant backmixing of the gases produced occurred. Our work focused on the cyclic operation of the oxygen carrier $La_{0.85}Sr_{0.15}FeO_3$ in a fluidized bed reactor, demonstrating that high conversions of CH_4 to synthesis gas can be achieved without co-feeding any other gas, such as O_2, CO_2 or steam. The selectivity towards synthesis gas was > 99%, irrespective of the reaction temperature employed. The oxygen carrier was cycled under redox conditions at temperatures up to 950°C for more than 50 h without operational problems, even at elevated pressure. No sophisticated synthesis techniques were employed, making the production of such low-surface area materials feasible also at larger scale, e.g. via spray-drying using metal oxide precursors. No segregation of crystalline phases was observed during cycling, suggesting that the oxygen carrier $La_{0.85}Sr_{0.15}FeO_{3-\delta}$ was always oxidized back to its thermodynamically most stable state, with only the non-stoichiometry δ varying depending on the oxidation atmosphere. On a particle scale, the oxygen carrier can therefore not "deactivate". Reduction and oxidation occurred largely in a single reaction step, and the conversion of CO_2 to CO was ~ 97% at temperatures > 900°C and limited by thermodynamics only (similarly, the conversion of steam to H_2 was measured ~ 94%). The oxygen storage capacity was > 10 wt.%, allowing to produce > 6 mol of synthesis gas during reduction and > 6 mol of H_2 or CO during oxidation per kg oxygen carrier. From a process point of view, the efficient integration of heat will be important, since the actual partial oxidation reaction of CH_4 with lattice oxygen is endothermic and the re-oxidation with CO_2 or steam is only mildly exothermic. Oxidation of the reduced oxygen carrier with air is highly exothermic and could potentially supply some of the heat required to sustain the reduction reaction, but also replenishes unselective oxygen for the conversion of CH_4 to synthesis gas.

Future work will focus on the effect of higher operating pressure, scale up and improving the oxygen carrier's reactivity for reduction by partially substituting Fe on the B-site of the perovskite. For example, using Al as substituent, the average conversion of CH_4 was > 90% in preliminary investigations, emphasizing the scope for improving these materials further.

Acknowledgements

References

[1] A. P. E. York, T. Xiao, M. L. H. G. Ã, *Top. Catal.* **2003**, *22*, 345–358.

[2] R. L. Keiski, S. Ojala, M. Huuhtanen, T. Kolli, K. Leiviskä, *Adv. Clean Hydrocarb. Fuel Process.* **2011**, 262–286.

[3] M. Fathi, E. Bjorgum, T. Viig, O. . Rokstad, *Catal. Today* **2000**, *63*, 489–497.

[4] R.-J. Li, C.-C. Yu, W.-J. Ji, S.-K. Shen, *Stud. Surf. Sci. Catal.* **2004**, *147*, 199–204.

[5] Q. Zafar, T. Mattisson, B. Gevert, *Ind. Eng. Chem. Res.* **2005**, *44*, 3485–3496.

[6] M. Rydén, A. Lyngfelt, T. Mattisson, *Fuel* **2006**, *85*, 1631–1641.

[7] F. He, Y. Wei, H. Li, H. Wang, *Energy & Fuels* **2009**, *23*, 2095–2102.

[8] L. F. de Diego, M. Ortiz, J. Adánez, F. García-Labiano, A. Abad, P. Gayán, *Chem. Eng. J.* **2008**, *144*, 289–298.

[9] M. Tang, L. Xu, M. Fan, *Appl. Energy* **2015**, *151*, 143–156.

[10] X. Zhu, K. Li, L. Neal, F. Li, *ACS Catal.* **2018**, *8*, 8213–8236.

[11] P. T. Krenzke, J. R. Fosheim, J. H. Davidson, *Sol. Energy* **2017**, *156*, 48–72.

[12] L. Zeng, Z. Cheng, J. A. Fan, L.-S. Fan, J. Gong, *Nat. Rev. Chem.* **2018**, *2*, 349–364.

[13] F. He, J. Chen, S. Liu, Z. Huang, G. Wei, G. Wang, Y. Cao, K. Zhao, *Int. J. Hydrogen Energy* **2019**, *44*, 10265–10276.

[14] X. Dai, C. Yu, Q. Wu, *J. Nat. Gas Chem.* **2008**, *17*, 415–418.

[15] D. Sastre, D. P. Serrano, P. Pizarro, J. M. Coronado, *J. CO2 Util.* **2019**, *31*, 16–26.

[16] K. Zhao, F. He, Z. Huang, G. Wei, A. Zheng, H. Li, Z. Zhao, *Korean J. Chem. Eng.* **2017**, *34*, 1651–1660.

[17] C. Huang, J. Wu, Y.-T. Chen, M. Tian, A. I. Rykov, B. Hou, J. Lin, C.-R. Chang, X. Pan, J. Wang, et al., *Commun. Chem.* **2018**, *1*, 55.

[18] J. A. Gómez-Cuaspud, C. A. Perez, M. Schmal, *Catal. Letters* **2016**, *146*, 2504–2515.

[19] Y. Zheng, K. Li, H. Wang, D. Tian, Y. Wang, X. Zhu, Y. Wei, M. Zheng, Y. Luo, *Appl. Catal. B Environ.* **2017**, *202*, 51–63.

[20] F. He, F. Li, *Energy Environ. Sci.* **2015**, *8*, 535–539.

[21] J. Zhang, V. Haribal, F. Li, *Sci. Adv.* **2017**, *3*, e1701184.

[22] S. Bhavsar, M. Najera, R. Solunke, G. Veser, *Catal. Today* **2014**, *228*, 96–105.

[23] D. D. Taylor, N. J. Schreiber, B. D. Levitas, W. Xu, P. S. Whitfield, E. E. Rodriguez, *Chem. Mater.* **2016**, *28*, 3951–3960.

[24] I. S. Metcalfe, B. Ray, C. Dejoie, W. Hu, C. de Leeuwe, C. Dueso, F. R. García-García, C.-M. Mak, E. I. Papaioannou, C. R. Thompson, et al., *Nat. Chem.* **2019**, DOI 10.1038/s41557-019-0273-2.

[25] E. Marek, W. Hu, M. Gaultois, C. P. Grey, S. A. Scott, *Appl. Energy* **2018**, *223*, 369–382.

[26] L. Liu, D. D. Taylor, E. E. Rodriguez, M. R. Zachariah, *Chem. Commun.* **2016**, *52*, 10369–10372.

[27] F. Mudu, B. Arstad, E. Bakken, H. Fjellvåg, U. Olsbye, *J. Catal.* **2010**, *275*, 25–33.

[28] L. Nalbandian, A. Evdou, V. Zaspalis, *Int. J. Hydrogen Energy* **2011**, *36*, 6657–6670.

[29] X. Dai, J. Cheng, Z. Li, M. Liu, Y. Ma, X. Zhang, *Chem. Eng. Sci.* **2016**, *153*, 236–245.

[30] A. Evdou, V. Zaspalis, L. Nalbandian, *Fuel* **2010**, DOI 10.1016/j.fuel.2009.09.028.

[31] K. Zhao, F. He, Z. Huang, A. Zheng, H. Li, Z. Zhao, *Chinese J. Catal.* **2014**, *35*, 1196–1205.

[32] K. Zhao, L. Li, A. Zheng, Z. Huang, F. He, Y. Shen, G. Wei, H. Li, Z. Zhao, *Appl. Energy* **2017**, *197*, 393–404.

[33] K. Zhao, F. He, Z. Huang, A. Zheng, H. Li, Z. Zhao, *Int. J. Hydrogen Energy* **2014**, *39*, 3243–3252.

[34] X. P. Dai, J. Li, J. T. Fan, W. S. Wei, J. Xu, *Ind. Eng. Chem. Res.* **2012**, *51*, 11072–11082.

[35] X. DAI, C. YU, R. LI, Q. WU, Z. HAO, *J. Rare Earths* **2008**, *26*, 76–80.

[36] H. V. Pralhad, H. Feng, M. Amit, L. Fanxing, *ChemSusChem* **2017**, *10*, 3282.

[37] L. A. Isupova, I. S. Yakovleva, G. M. Alikina, V. A. Rogov, V. A. Sadykov, *Kinet. Catal.* **2005**, *46*, 729–735.

[38] T. Li, R. S. Jayathilake, D. D. Taylor, E. E. Rodriguez, *Chem. Commun.* **2019**, *55*, 4929–4932.

[39] F. He, X. Li, K. Zhao, Z. Huang, G. Wei, H. Li, *Fuel* **2013**, *108*, 465–473.

[40] C. Huang, J. Wu, Y.-T. Chen, M. Tian, A. I. Rykov, B. Hou, J. Lin, C.-R. Chang, X. Pan, J. Wang, et al., *Commun. Chem.* **2018**, *1*, 55.

[41] V. M. Goldschmidt, *Naturwissenschaften* **1926**, *14*, 477–485.

[42] O. Mihai, D. Chen, A. Holmen, *Ind. Eng. Chem. Res.* **2011**, *50*, 2613–2621.

[43] G. Voitic, V. Hacker, *RSC Adv.* **2016**, *6*, 98267–98296.

[44] F. Li, L. Zeng, L. G. Velazquez-Vargas, Z. Yoscovits, L.-S. Fan, *AIChE J.* **2010**, *56*, 2186–2199.

[45] A. Tong, S. Bayham, M. V Kathe, L. Zeng, S. Luo, L. S. Fan, *Appl. Energy* **2014**, *113*, 1836–1845.

[46] C. Y. Wen, Y. H. Yu, *AIChE J.* **1966**, *12*, 610–612.